

Comparisons Among EIT Data Collection Techniques and Reconstruction Algorithms

Stefano Pisa, Erika Pittella, and Emanuele Piuzzi

Dept. of Information Engineering, Electronics and Telecommunications (DIET)
Sapienza University of Rome, via Eudossiana, 18, 00184, Rome, Italy
stefano.pisa@uniroma1.it, erika.pittella@uniroma1.it, emanuele.piuzzi@uniroma1.it

Abstract — Electrical Impedance Tomography (EIT) is an imaging technique that aims to reconstruct the spatial electrical conductivity distribution in sections of the human body. In this paper, in order to solve the EIT forward and inverse problems, a finite difference approach to the solution of Maxwell's equations and the Newton-Raphson algorithm have been employed, respectively. In particular, the inverse problem has been solved using the Tikhonov regularization with various choices of the regularization matrix. Moreover, different data collection methods have been tested on simulated measurements. The obtained results have been compared based on the average deviation of the estimated conductivity distribution with respect to the reference one. The reconstruction procedure has been validated through a comparison with the EIDORS open source software. The best image reconstruction has been obtained by using the neighboring data collection method with null regularization matrix, and using the truncated singular value decomposition to perform the matrix inversion. Moreover, the cross and opposite data collection methods showed better performance than the neighboring one in the presence of a random noise added to the measured signal, while the opposite method evidenced the best results with respect to electrode positioning uncertainties.

Index Terms — Electrical impedance tomography, finite difference method, Newton-Raphson algorithm.

I. INTRODUCTION

Electrical impedance tomography (EIT) is an imaging technique, which leads to an estimation of the spatial electrical conductivity distribution in a section of the human body, by injecting currents and measuring voltages between pairs of electrodes distributed upon the body surface [1-3]. Compared with standard biomedical imaging techniques (e.g., Magnetic Resonance Imaging or Computed Tomography), the EIT has lower spatial resolution [4] but many advantages, mainly a simpler and cheaper experimental set-up, and the total absence of health risks for the patient. In particular, the typical frequencies and amplitudes of the driving currents, from

10 kHz to 100 kHz, and lower than 10 mA, respectively, cannot interfere with the normal electrophysiological activities of excitable biological tissues. Typical EIT applications are the dynamic monitoring of respiratory and cardiac activities, the study of cerebral hemodynamics, stomach emptying, and fracture healing [1-3].

To reconstruct the spatial electrical conductivity distribution in the investigated section, EIT uses reconstruction algorithms requiring two data sets. One data set is represented by the measured voltages collected on the surface of the real body, and the other is constituted by the computed voltages on the surface of a body model with the same boundary of the real one and with an a priori established conductivity distribution.

In order to compute the voltages on the body surface, the forward problem, namely Poisson's equation with known boundary conditions, needs to be solved. For the solution of the EIT forward problem, various numerical techniques have been proposed. The finite element method (FEM) is the mostly used technique [1, 5], but finite difference (FD) methods have been also suggested [6-8].

With reference to reconstruction algorithms, the first to be developed were the back projection and the sensitivity methods [9-11], but today the most used is the modified Newton-Raphson method [12]. This method follows the nonlinear least square approach applied to the minimization of an error function. The minimization process leads to an updating equation, for the discrete conductivity distribution, involving the computation of the Jacobian matrix of the forward operator. Moreover, the solution of the conductivity updating linear system needs the inversion of a quadratic form of the Jacobian, which is an ill-conditioned matrix. In order to improve the conditioning of this matrix, Tikhonov regularization method [13] can be applied with different choices of the regularization matrix [8, 13-17].

For the measurement collection, a given number (E) of equally spaced electrodes are placed upon the surface of the object under investigation. In some techniques, like the neighboring [1], the opposite (polar) [2], or the cross [2], a current is injected through a pair of electrodes

and voltages are measured between the remaining pairs. Other techniques apply a current through all the electrodes and measure the resulting voltages at the same electrodes using one of them as reference [1]. In the latter approach, more data are collected with respect to the former methods, with the disadvantage that voltage measurements are dependent on the unknown contact impedance existing between skin and electrode.

Due to the availability of multiple reconstruction algorithms and data collection techniques, the question arises about the best choice for the implementation of an experimental set-up. In [12] many reconstruction algorithms have been compared, evidencing the superior capability of the modified Newton-Raphson method with regularization. Various data collection techniques have been compared with respect to their performance and resolution, by using a modified back projection technique, and the superiority of the neighboring method has been evidenced [18]. However, in [12] and [18] only very simplified models of the investigated region have been considered, not allowing a realistic study of the performance of the various techniques. Moreover, in order to thoroughly test a technique it is also important to check its robustness with respect to sources of error like the random noise affecting the measured data and the misalignment between measurement electrodes on the subject and on the numerical phantom.

For these reasons, in this work an anatomical model will be considered. The neighboring, cross and opposite methods of data collection will be compared by using a regularized version of the Newton-Raphson method with various choices of the regularization matrix. A FD solution of Maxwell's equations in quasi-static conditions, namely the admittance method, will be used for the solution of the direct problem involved in EIT. The effect of noise sources and electrode misalignment on the reconstruction algorithms will be investigated. Preliminarily, the proposed reconstruction procedure will be validated by studying a canonical body model constituted by a square geometry with a square anomaly and comparing the results with those achieved by using the EIDORS open source software [19].

II. METHODS AND MODELS

A. Considered models

Two thorax models have been considered in this study. The first is a simple square geometry with a conductivity of 0.12 S/m filled with a square central anomaly with conductivity equal to 0.24 S/m (see Fig. 1 (a)). These two values roughly correspond to the average conductivity of the thorax and of the deflated lung, respectively.

The second is an anatomical thorax model (45×45 pixels, 1 cm side) obtained by under-sampling a section, at the thorax level, of the Visible Human (VH) data set [20], and it comprises skin/fat, muscle, bone, lung, and

heart tissues. The conductivity values of the various tissues at the frequency of 50 kHz have been taken from literature data [21]. For skin/fat, heart, muscle, and bone, these values are 0.03, 0.45, 0.35, and 0.02, S/m, respectively. Finally, for the lungs a conductivity value of 0.25 S/m has been assumed corresponding to the deflated lung condition. Figure 1 (b) shows a conductivity map of the considered section.

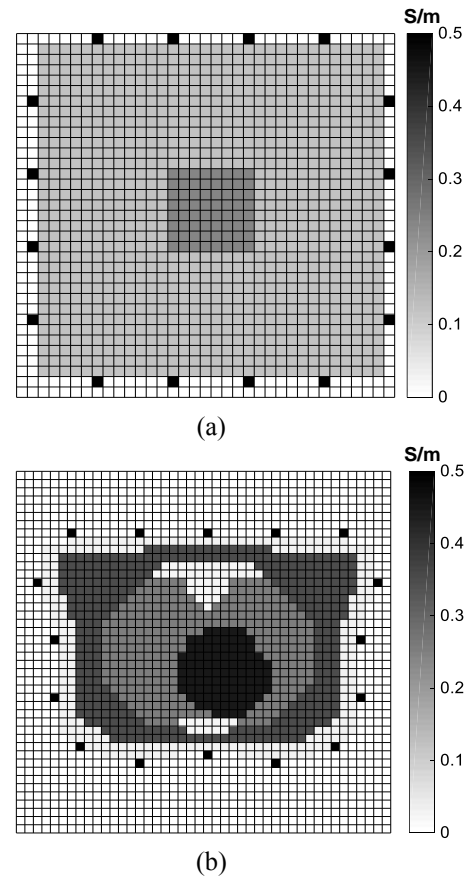


Fig. 1. Conductivity map of the square geometry (a) and of the under-sampled visible human section at thorax level (b). Black squares represent the electrodes.

B. Data collection methods

Three data collection techniques have been considered, namely the neighboring, the cross, and the opposite methods. In all cases, 16 equally-spaced electrodes are placed upon the surface of the body, as shown in Fig. 2. Concerning the neighboring method, the current is injected through a pair of adjacent electrodes (1 and 2 in Fig. 2 (a)) and voltages are measured between the remaining different pairs of adjacent electrodes [1]. Then, the driving pair is changed and the measuring process is repeated, until each pair has been used as driving. In this way, $16 \times 13 = 208$ potential differences are collected, but only 104 of these are linearly independent due to the reciprocity theorem.

In the cross method, the current is injected through a couple of odd electrodes (1 and 3 in Fig. 2 (b)) and voltages are measured between the other electrodes, except the current ones, with electrode 2 chosen as voltage-reference [2]. Then, the current is applied to the remaining odd electrodes (1-5, 1-7 etc.) and voltages are measured using the electrode 2 as voltage reference. In this manner $7 \times 13 = 91$ potential differences are collected. The measurement sequence is then repeated applying currents through even electrodes and measuring with the electrode 1 as voltage reference. A total number of

182 measurements is finally collected, with only 104 independent.

In the opposite method, current is injected through a pair of diametrically opposed electrodes (1-9 in Fig. 2 (c)) and voltages are measured on each electrode, with respect to a reference node adjacent to the current-injecting electrode [2]. Then, the driving pair is switched to the next pair of opposite electrodes in the clockwise direction, changing the voltage reference node accordingly. Here again 208 potential differences are collected, but only 104 of these are linearly independent for reciprocity.

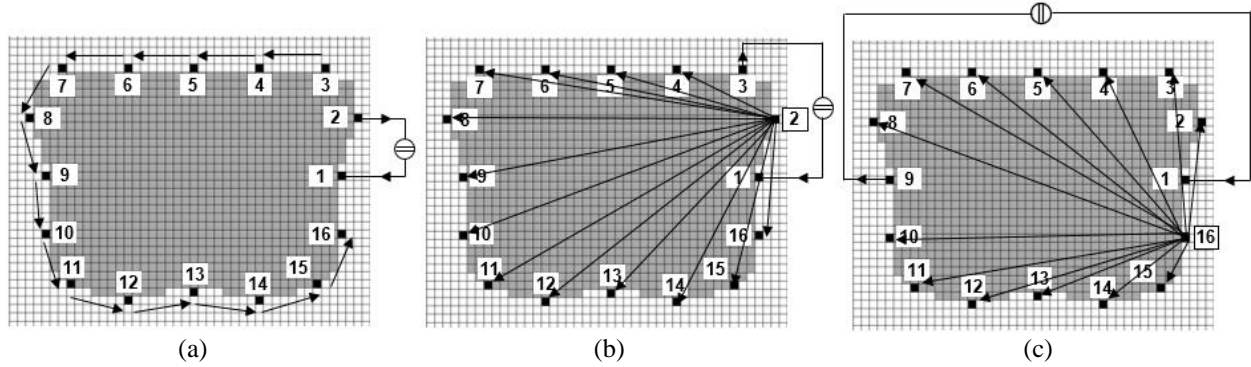


Fig. 2. Data collection techniques: neighboring (a), cross (b), and opposite (c).

C. The admittance method

In the EIT forward problem the section is discretized in a bi-dimensional grid of N square (homogeneous) cells and the continuous conductivity distribution is discretized in a real matrix \underline{C} whose generic element $c(x,y)$ is the discretized conductivity value at the grid nodes (cell center). The admittance method is a finite difference approach to the solution of Maxwell's equations in quasi-static conditions [22]. In this method, the discretized domain is modeled as a network of admittances (see Fig. 3) and the application of Kirchhoff's current law gives rise, for each cell, to the following linear equation:

$$V(x, y) = \frac{1}{Y_{x^+} + Y_{x^-} + Y_{y^+} + Y_{y^-}} \cdot \left(Y_{x^+} V(x + \Delta x, y) + Y_{x^-} V(x - \Delta x, y) + Y_{y^+} V(x, y + \Delta y) + Y_{y^-} V(x, y - \Delta y) - I_{ie} \right), \quad (1)$$

where $V(x, y)$ represents the discretized potential at the (x, y) node, I_{ie} is the known forcing term (source) of the equation, and the admittance terms are computed, looking for example, at Y_{x^+} , as follows:

$$Y_{x^+} = c_{x^+} \frac{\Delta y \Delta z}{\Delta x} = \frac{2 c(x,y) \cdot c(x+\Delta x, y)}{c(x,y) + c(x+\Delta x, y)} \frac{\Delta y \Delta z}{\Delta x}. \quad (2)$$

The resulting linear system of N equations in N unknowns can be solved by using either an iterative or a direct approach.

In the iterative technique, an estimation of the potential $V^{n+1}(x, y)$ of the (x, y) cell at the $(n+1)^{\text{th}}$ step can be obtained by adding to the previous estimation,

$V^n(x, y)$, a correction term as follows:

$$V^{n+1}(x, y) = V^n(x, y) + \alpha [V(x, y) - V^n(x, y)], \quad (3)$$

where $1 < \alpha < 2$ is called the over-relaxation parameter and $V(x, y)$ is given by (1). The iterative procedure stops when, for every cell, the following condition is met:

$$|V^{n+1}(x, y) - V^n(x, y)| < \varepsilon, \quad (4)$$

with ε an arbitrarily small positive quantity.

In the direct approach, in order to obtain linearly independent equations, the $(N \times N)$ system matrix described by (1), which associates a unique integer number to each cell, is reduced to a $(N-1 \times N-1)$ matrix by choosing a reference cell with respect to which every voltage is computed. This system can be written in a matrix form as:

$$\underline{Y} \cdot \underline{V} = \underline{I}, \quad (5)$$

where \underline{V} is the $(N-1 \times 1)$ vector of the unknown discrete voltage distribution, \underline{I} is the $(N-1 \times 1)$ vector of the known discrete current distribution, and \underline{Y} is the $(N-1 \times N-1)$ admittance matrix, each row of which has all zero elements, except usually for five of them. By inverting \underline{Y} , the solution vector \underline{V} to the linear system (5) can be obtained.

To collect the computed voltages a number P (with P equal to 16 or 14, see Section II.B) of current injection patterns are applied through the electrodes placed upon the body surface. All the implemented reconstruction algorithms need to compute, for each injection pattern, a

number G (typically 13) of voltage differences between well-defined electrode pairs. The computed voltages are stored into an $(M \times 1)$ vector $\underline{g}^{\text{comp}}$ ($M = P \cdot G$).

In order to collect the measured voltages, the same current injection patterns used in the simulations are applied through electrodes placed upon the surface of the real body whose conductivity has to be estimated. In this work, the measured voltages have been obtained through simulations performed on the considered conductivity distributions (see Fig. 1) by using the admittance method, and stored into the $(M \times 1)$ vector $\underline{g}^{\text{meas}}$.

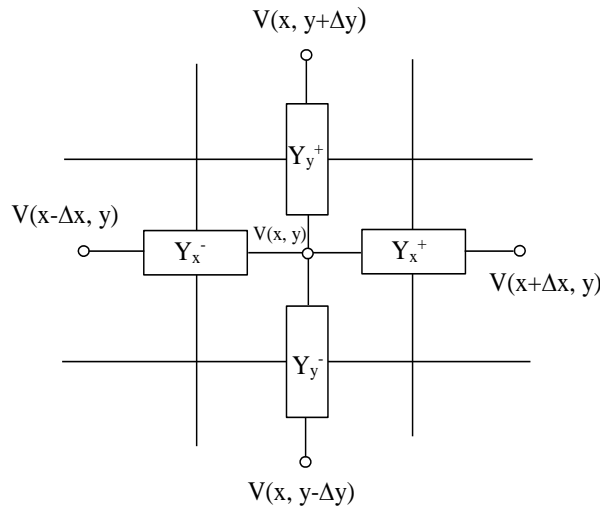


Fig. 3. Network of admittances modeling the discretized domain.

D. The Newton-Raphson reconstruction algorithm

The Newton-Raphson (N&R) method has been specifically developed for problems whose mathematical models are non-linear and it has been extensively described by Yorkey [12]. The aim of this technique is to minimize an error function $\Phi(\underline{e})$, where \underline{e} is the difference vector between the voltages measured on the real conductivity distribution and those calculated on a known, discretized conductivity distribution. $\Phi(\underline{e})$ is defined as:

$$\Phi(\underline{e}) = \frac{1}{2} \left\| \underline{g}^{\text{comp}}(\underline{c}) - \underline{g}^{\text{meas}} \right\|^2, \quad (6)$$

where $\| \cdot \|^2$ represents the standard 2-norm of a vector. Starting from (6), it can be shown that the conductivity update distribution at k^{th} step is approximately given by:

$$\underline{\Delta c}^k = - \left[\underline{J}_k^T \underline{J}_k \right]^{-1} \cdot \underline{J}_k^T \cdot \left[\underline{g}^{\text{comp}}(\underline{c}^k) - \underline{g}^{\text{meas}} \right], \quad (7)$$

where $\underline{J}_k = \underline{J}(\underline{c}^k)$ is the $(M \times N)$ Jacobian matrix of the forward transformation $\underline{g}^{\text{comp}}(\underline{c}^k)$ defined as [1]:

$$\underline{J}(\underline{c}) = \frac{\partial \underline{g}^{\text{comp}}(\underline{c})}{\partial \underline{c}}. \quad (8)$$

Finally, the conductivity at the $(k+1)^{\text{th}}$ step is given by:

$$\underline{c}^{k+1} = \underline{c}^k + \underline{\Delta c}^k. \quad (9)$$

This procedure is repeated until $\Phi(\underline{e})$ is less than an a priori chosen value.

The updating Equation (7) of the N&R algorithm needs the inversion of the matrix $\underline{J}_k^T \underline{J}_k$, which is a very ill conditioned matrix. The best way to solve this problem is to use regularization techniques, like the one proposed by Tikhonov [13].

The basic idea is to modify the functional $\Phi(\underline{e})$ in (6) as follows:

$$T(\underline{c}) = \frac{1}{2} \left\| \underline{g}^{\text{comp}}(\underline{c}) - \underline{g}^{\text{meas}} \right\|^2 + \alpha \left\| \underline{L} \cdot \underline{c} \right\|^2, \quad (10)$$

where α is called the regularization parameter and \underline{L} is a real banded regularization matrix.

For the iterative linearized problem, the conductivity updating term becomes [3]:

$$\underline{\Delta c}^k = - \left[\underline{J}_k^T \underline{J}_k + \alpha \underline{L}^T \underline{L} \right]^{-1} \cdot \underline{J}_k^T \left[\underline{g}^{\text{comp}}(\underline{c}^k) - \underline{g}^{\text{meas}} \right] - \alpha \underline{L}^T \underline{L} \underline{c}^k. \quad (11)$$

In this work, various choices for \underline{L} have been implemented. First of all the $\underline{L} = \underline{0}$ null matrix has been considered (L0 condition). In this case, to perform the matrix inversion, a suitable technique is the singular value decomposition (SVD) [23]. Let \underline{A} be the matrix to be inverted, \underline{U} the matrix of the eigenvectors of $\underline{A}^T \underline{A}$, \underline{V} the matrix of the eigenvectors of $\underline{A} \underline{A}^T$, and $\underline{\Sigma}$ the matrix whose main diagonal contains the square root of the eigenvalues of $\underline{A}^T \underline{A}$ in descending order; the following result is obtained:

$$\underline{A}^{-1} = \underline{V} \underline{\Sigma}^{-1} \underline{U}^T. \quad (12)$$

In EIT problems, the truncated SVD (TSVD) is generally employed. In the TSVD, only the largest singular values (beyond a certain established tolerance) are considered, setting to zero the smaller ones (with the corresponding singular vectors). This choice avoids to introduce "noise" in the solution produced by the small singular values.

Another considered choice is $\underline{L} = \underline{I}$ where the regularization matrix is equal to the identity matrix (LI condition). Finally, the matrix \underline{L} has been taken as a discretization of the second order differential operator ∇^2 (LD2 condition). In the latter cases, the matrices to be inverted are all full rank and standard LU factorization can be applied for their inversion.

III. RESULTS

The Newton-Raphson algorithm has been implemented in Fortran 90 language and the IMSL libraries have been used for the classical and generalized inversion of the involved matrices.

In order to quantitatively compare the reconstructed voltages, a weighed version of the functional defined in

(6) for the k^{th} step of iteration has been used, given by:

$$e_g^k = \frac{[\underline{g}^{\text{comp}}(\underline{c}^k) - \underline{g}^{\text{meas}}]^T \cdot [\underline{g}^{\text{comp}}(\underline{c}^k) - \underline{g}^{\text{meas}}]}{(\underline{g}^{\text{meas}})^T \cdot \underline{g}^{\text{meas}}} \times 100 \quad (13)$$

Moreover, in order to better quantify the accuracy of the reconstructed images, a second error, namely the percentage average deviation of the estimated conductivity distribution \underline{c}^k with respect to the real one \underline{c} , has been defined as:

$$e_c^k = \frac{[\underline{c} - \underline{c}^k]^T \cdot [\underline{c} - \underline{c}^k]}{\underline{c}_{\text{av}}^T \cdot \underline{c}_{\text{av}}} \times 100, \quad (14)$$

where $\underline{c}_{\text{av}}$ is a vector with elements equal to the arithmetic average of \underline{c} .

A. Numerical codes validation

The square model with a square central anomaly shown in Fig. 1 (a) has been studied by using the neighboring data collection method and LI reconstruction algorithm with $\alpha = 10^{-3}$ and background conductivity equal to 0.12 S/m. The same problem has been solved with the EIDORS absolute solver with hyperparameter equal to 10^{-3} and background conductivity equal to 0.12 S/m [19].

Figure 4 shows the simulated electrode voltages, for the first injection couple, obtained by using as direct solver the FD method proposed in this work, compared with those achieved by using the FEM method implemented in EIDORS. A very good agreement between the two techniques can be observed.

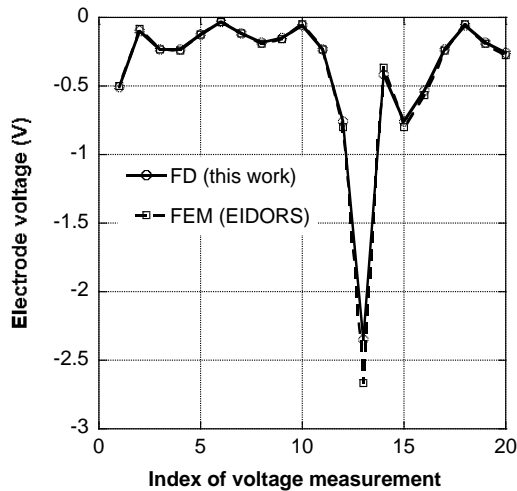


Fig. 4. Electrode voltages for the square geometry with square anomaly computed by using the FD method and the FEM method implemented in EIDORS.

The reconstructed conductivity distribution obtained

with EIDORS is reported in Fig. 5 (a) and the one obtained by using the approach proposed in this paper in Fig. 5 (b). The two reconstructions look very similar. In fact, the application of (14) gives a reconstruction error of 0.9697% and 0.9696% for the EIDORS and the proposed method, respectively.

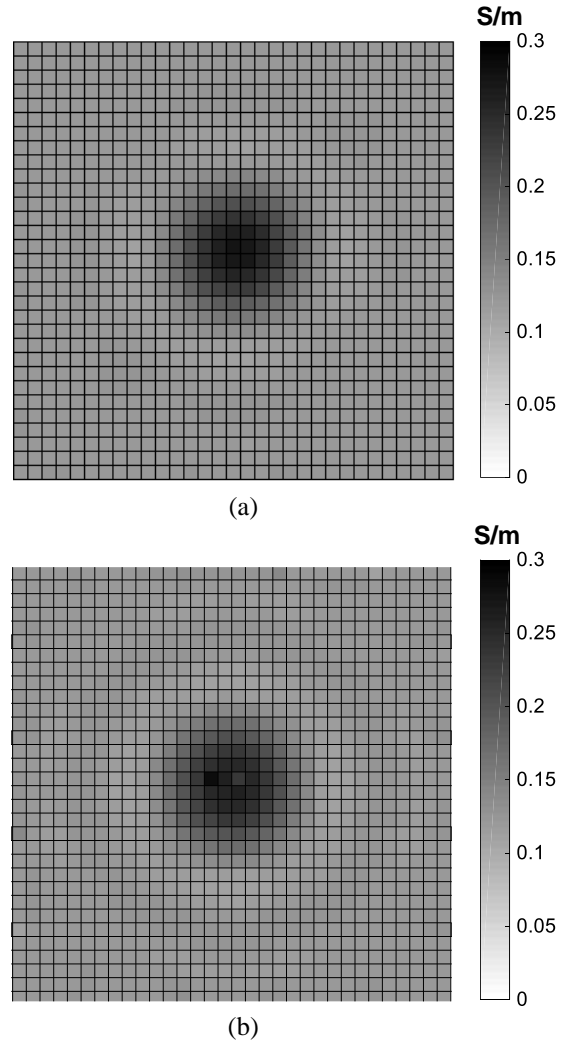


Fig. 5. Reconstructed conductivity maps for the square geometry by using EIDORS (a), and the technique proposed in this paper (b).

With reference to the best case for the voltage driven approach (opposite with L0), Fig. 6 shows the reconstructed images and voltages. In particular, Fig. 6 (a) shows the reconstructed image after seven iterations ($\epsilon_c = 22.59\%$), while Fig. 6 (b) reports a comparison between the simulated voltage measurements and the reconstructed voltages after seven steps ($\epsilon_g = 0.0001\%$). Figure 7 (b) shows that after seven iterations of the opposite L0 method, the reconstructed voltage

measurements almost perfectly match the measurement on the phantom, but a considerable error on the reconstructed image is present. Concerning the voltage driven approach, the best-reconstructed image is obtained by using the cross method with LI ($\varepsilon_c = 18.07\%$), in this case the error on the voltage is very small ($\varepsilon_g = 0.0098\%$) but higher than the previous case.

By using the image driven approach, the best image reconstruction is achieved by the neighboring method with L0 (see Fig. 7 (a)). The superiority of this image reconstruction with respect to the previous ones is evident. By comparing this figure with Fig. 1 (b), the good contour identification of all the thorax tissues is well evidenced.

B. Comparisons among different data collection and reconstruction algorithms

In the following, the anatomical thorax model has been considered and two sets of simulations have been performed. Each set contains simulation performed by using L0, LI and LD2 reconstruction methods and the neighboring, cross, and opposite data collection techniques.

In the first set (called voltage driven) the background conductivity, and the tolerance or the regularization parameter have been optimized in order to achieve the lowest error as defined in (13), while in the second set (called image driven) the parameters have been

optimized in order to achieve the lowest error as defined in (14). The first approach is representative of the situation encountered in realistic experiments, where the goal of the reconstruction procedure is to achieve a distribution of the simulated voltages between the electrodes placed on the body surface as close as possible to the measured one. The second approach, instead, gives a better evaluation of the ability of the various techniques in reconstructing the internal geometry of the body.

The results obtained with the voltage driven approach are reported in Table 1. The table shows that the lowest reconstruction error is obtained by using the opposite method with L0 (0.0001%), while the highest error is obtained with the neighboring method with LI (0.1745%). In these simulations, the image reconstruction errors (as defined in (14)) are always higher than 18%. It is worth noting that the method with the lowest voltage reconstruction error gives rise to a very high image reconstruction error (22.59%). The table also shows that in all the situations the best background conductivity is equal to 0.12 S/m.

The results obtained with the image driven approach are reported in Table 2. In this case, the lowest reconstruction error is obtained by using the neighboring method with L0 (13.44%), while the highest error is obtained with the opposite method with LD2 (23.55%). Moreover, in all cases the best results are obtained by using a background conductivity equal to 0.06 S/m.

Table 1: Parameters that give rise to the best e_g^k for the L0, LI and LD2 reconstruction methods and the neighboring, cross, and opposite data collection techniques for the voltage driven approach. In the table the e_c^k obtained at the last step are also reported

		L0	LI	LD2
Neighboring Method	σ_{BG}	0.12	0.12	0.12
	Tol	$1.0e^{-2}$	/	/
	α	/	$2.0e^{-1}$	$1.0e^{-2}$
	e_g^N	0.0279%	0.1745%	0.0204%
	e_c^N	24.32%	18.97%	18.16%
Cross Method	σ_{BG}	0.12	0.12	0.12
	Tol	$1.0e^{-2}$	/	/
	α	/	$2.0e^{-1}$	$5.0e^{-1}$
	e_g^N	0.0004%	0.0098%	0.0107%
	e_c^N	21.31%	18.07%	19.31%
Opposite Method	σ_{BG}	0.12	0.12	0.12
	Tol	$1.0e^{-2}$	/	/
	α	/	$5.0e^{-2}$	$5.0e^{-2}$
	e_g^N	0.0001%	0.0167%	0.0035%
	e_c^N	22.59%	18.90%	19.84%

Table 2: Parameters that give rise to the best e_c^k for the L0, LI and LD2 reconstruction methods and the neighboring, cross, and opposite data collection techniques for the image driven approach. In the Ttble the e_g^k obtained at the last step are also reported

		L0	LI	LD2
Neighboring Method	σ_{BG}	0.06	0.06	0.06
	Tol	1.0e-4	/	/
	α	/	1.0e-3	5.0e-4
	e_c^N	13.44%	15.98%	23.37%
	e_g^N	1.00%	2.98%	1.91%
Cross Method	σ_{BG}	0.06	0.06	0.06
	Tol	1.0e-4	/	/
	α	/	1.0e-3	5.0e-4
	e_c^N	15.52%	17.19%	22.61%
	e_g^N	0.09%	3.21%	3.34%
Opposite Method	σ_{BG}	0.06	0.06	0.06
	Tol	1.0e-4	/	/
	α	/	1.0e-3	5.0e-4
	e_c^N	16.92%	15.50%	23.55%
	e_g^N	0.08%	0.38%	2.72%

C. Effects of noise and electrode misalignment

The above reported image reconstructions have been performed by neglecting the presence of noise on the measured data and supposing that measured and simulated data are collected by means of electrodes placed in the same positions. In an experimental set up the measuring apparatus introduces a random noise. Moreover, measurements are performed by placing the electrodes on a belt in approximately equally spaced positions, while the simulations are performed on a phantom that roughly mimics the real electrode positioning.

In order to investigate the relevance of the random noise on the reconstructions, the simulated measurements have been modified by adding to the voltage data (g^{meas}) a Gaussian voltage noise with zero mean and with various levels of standard deviation. Figure 8 shows the obtained image reconstruction error as a function of the noise standard deviation, by considering three data collection methods and the L0 reconstruction algorithm. The figure evidences that for low noise levels the neighboring method allows the best image reconstruction while, increasing the noise standard deviation, the cross and opposite methods give better results. This is probably because, as evidenced in Fig. 6 (b), the opposite technique gives rise to higher electrode voltages that are less influenced by noise. On the same figure, the image

reconstruction error achieved with the opposite method with LI is also reported. This curve shows a strong increase, with the noise standard deviation, of the error at low noise levels. This result suggests that the L0 technique is more efficient in reducing the effect of noise.

In order to study the effect of the electrode misalignment, a set of reconstructions has been performed by using simulated measurement data obtained by shifting of one cell (about 1 cm) a single electrode and evaluating the image reconstruction error with simulations performed with the electrode in its initial position. In all the simulations, the L0 reconstruction method with a background conductivity of 0.06 S/m has been used

These simulations have been repeated for all the sixteen electrodes, by considering the neighboring, cross, and opposite data collection techniques.

The variations of the image reconstruction error with respect to the aligned case are reported in Fig. 9. The figure shows that the variations are generally lower than 2%. However, by evaluating the average over the sixteen positions, values of 1.425%, 1.474% and 1.097% are obtained for the neighboring, cross and opposite methods, respectively. In conclusion, this analysis seems to indicate that the opposite method is the most robust data collection technique with respect to the electrode misalignment.

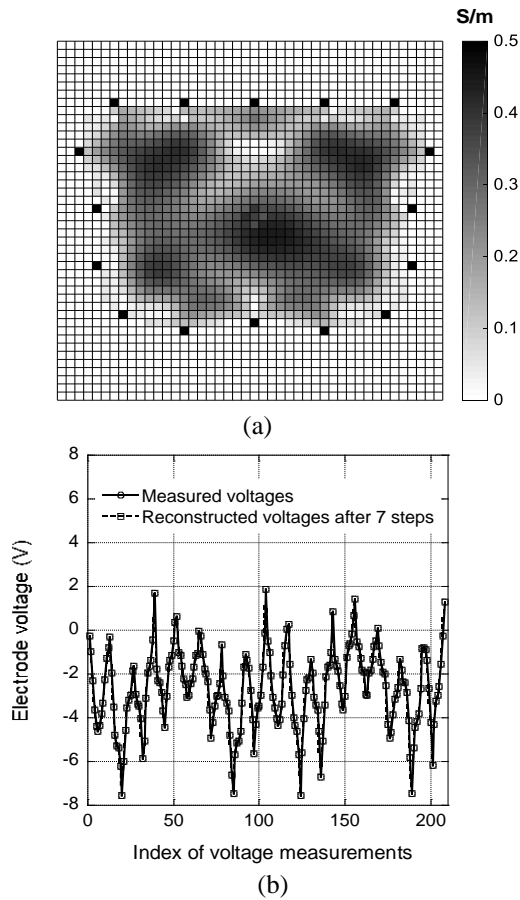


Fig. 6. Opposite method with L0: (a) conductivity distribution, and (b) comparison between measured and simulated electrode voltages after seven iterations.

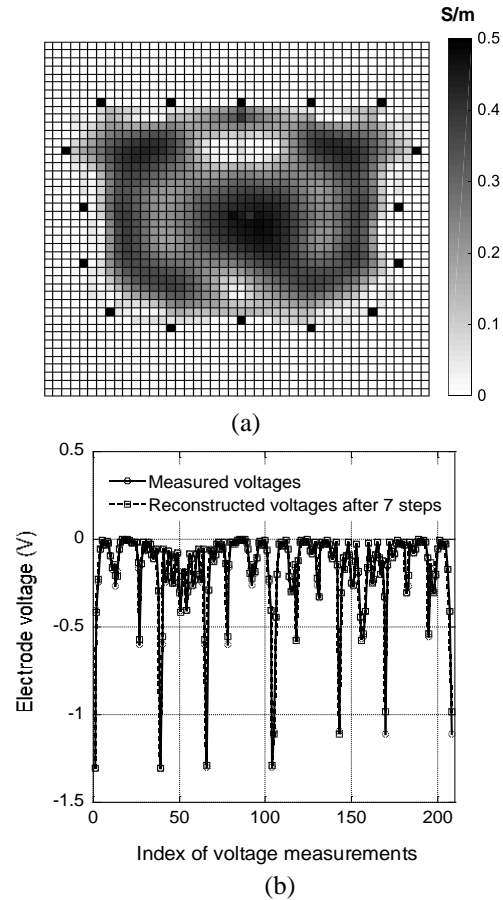


Fig. 7. Neighboring method with L0: (a) conductivity distribution, and (b) comparison between measured and simulated electrode voltages after seven iterations.

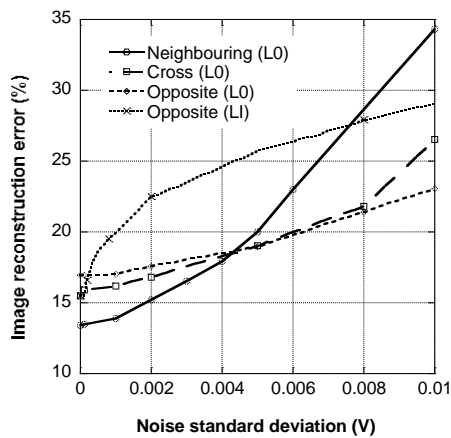


Fig. 8. Image reconstruction error as a function of the noise standard deviation.

IV. CONCLUSION

In this paper, the mathematical background and the implementation details of the admittance and Newton-

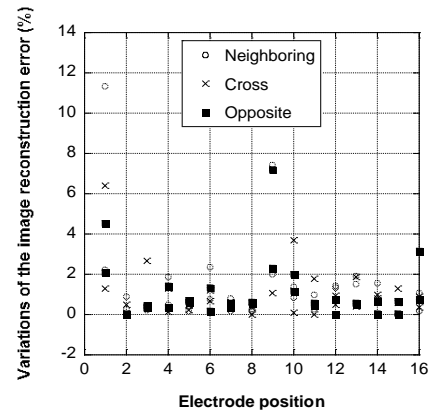


Fig. 9. Variations of the image reconstruction error due to electrode misalignment as a function of the electrode position.

Raphson methods, applied to the EIT problem, have been described.

The reconstruction procedure has been validated

through a comparison with the EIDORS open source software. The obtained results show that the FD method gives electrode voltage distributions in very good agreement with the FEM method implemented in EIDORS. Moreover, the errors on the image reconstruction are comparable. It is worth to be noted that FEM is a very accurate technique but needs complex mesh generators. On the contrary, the use of FD methods with square cells in a Cartesian reference system makes the modeling and computation of voltage distributions easy and accurate. Moreover, the memory occupation of FEM technique grows as the square of the number of cells while the memory occupation of the FD technique grows linearly with the cell number. This makes the FD a preferred choice for 3D problems with a high number of cells [24].

It is worth noting that for the considered EIT problem the FD method has been solved by considering only the real part of the tissue conductivity. However, the same method can also be applied by considering both the real and the imaginary part (related to the permittivity) of the conductivity of the tissues. This last approach could be useful in applications where it is necessary to increase the operating frequency. Moreover, by adding to the circuit in Fig. 3 current generators related to the vector potential distribution [22] the same method can be used to study the magnetic detection electrical impedance tomography [25, 26].

Various reconstruction algorithms and data collection techniques have been compared by using a realistic model instead of the simplified square or cylindrical models previously considered in papers where different EIT techniques were compared [12, 18, 27]. In fact, as evidenced by Grychtol et al. [28], for testing inversion algorithms and data collection techniques it is important to use anatomical, morphologically accurate, models. This is another advantage of the FD method that allows to study realistic, pixel based, anatomical human models easily imported in the FD grid. Recently, realistic human models, generated from the visible human data set [20] to be used with FEM mesh, have been proposed [29, 30]. However, these models take into account only the external body surface and a few organs. The FD method, on the contrary, by using the full pixel based models, can consider the high variability of the human anatomy.

The reconstruction problem has been solved using Tikhonov regularization with various choices of the regularization matrix and of the data collection method. The obtained results have been compared by using the percentage deviation of the simulated electrode voltages with respect to the measured one and the percentage deviation of the evaluated conductivity distribution with respect to the real one. By using the first metric to stop the simulations, very low voltage reconstruction errors are achieved but this does not give rise to good image reconstructions, as compared with those obtained by

using the image driven approach. In particular, in the performed study the best image reconstruction has been obtained by using the neighboring method with null regularization matrix and using the truncate singular value decomposition to perform the matrix inversion. In conclusion, the better reconstruction properties of the neighboring technique with respect to the other approaches, previously evidenced by using simplified body models and a back projection algorithm [18, 31], have been confirmed, in the present paper, by using a more realistic anatomical model and various forms of the Newton-Raphson algorithm.

Various inversion and data collection techniques have been compared in terms of robustness to random noise and electrode misalignments. To this end, the cross and opposite methods show better performance with respect to the neighboring method in the presence of a random noise over imposed to the measured signals. This is probably because the cross and opposite techniques give rise to higher electrode voltages, that are less influenced by the noise. This result is in agreement with literature data [18] achieved on simplified circular geometries. The opposite method showed the best performance with respect to electrode positioning uncertainties. A possible explanation is the uniform field distribution produced by the electrodes excitation used in the opposite technique that is less influenced by an electrode misalignment.

Finally, it is important to note that the EIT reconstructed images lack a good resolution and give only a rough representation of the body section. However, their acquisition is very fast thus allowing, for example, the monitoring of lung movement and conductivity variations during the breathing cycle [32].

REFERENCES

- [1] J. G. Webster, *Electrical Impedance Tomography*. Adam Hilger, Bristol, New York, 1990.
- [2] J. Malmivuo and R. Plonsey, *Bioelectromagnetism: Principles and Application of Bioelectric and Biomagnetic Fields*. Oxford University Press, New York, 1995.
- [3] D. S. Holder, *Electrical Impedance Tomography: Methods, History and Applications*. Institute of Physics, Great Britain, CRC Press, 2005.
- [4] A. D. Seagar, D. C. Barber, and B. H. Brown, "Theoretical limits to sensitivity and resolution in impedance imaging," *Clin. Phys. Physiol. Meas.*, vol. 8(A), pp. 13-31, 1987.
- [5] T. M. Murai and Y. Kagawa, "Electrical impedance computed tomography based on a finite element model," *IEEE Transactions on Biomedical Engineering*, vol. 32, no. 3, pp. 177-184, 1985.
- [6] R. P. Patterson and J. Zhang, "Evaluation of an EIT reconstruction algorithm using finite difference human thorax models as phantoms," *Physiol. Meas.*,

- vol. 24, pp. 467-475, 2003.
- [7] P. Kauppinen, J. Hyttinen, P. Laarne, and J. Malmivuo, "A software implementation for detailed volume conductor modelling in electrophysiology using finite difference method," *Computer Methods and Programs in Biomedicine*, vol. 58, pp. 191-203, 1999.
- [8] D. Romano, S. Pisa, and E. PiuZZi, "Implementation of the Newton-Raphson and admittance methods for EIT," *International Journal of Bioelectromagnetism*, vol. 1, pp. 12-20, 2010.
- [9] C. C. Barber and B. H. Brown "Imaging spatial distributions of resistivity using applied potential tomography," *Electronics Letters*, vol. 19, no. 22, pp. 933-935, 1983.
- [10] L. Hao, L. Xu, B. Yang, and G. Li, "Image reconstruction based on the anatomical information for magnetic resonance electrical impedance tomography," *Applied Computational Electromagnetics Society Journal*, vol. 31, no. 6, pp. 700-705, 2016.
- [11] D. Romano, S. Pisa, E. PiuZZi, and L. Podestà, "A comparison between back projection and sensitivity methods in EIT reconstruction problems," *In Proceedings of 19th International Zurich Symposium on Electromagnetic Compatibility*, Singapore, pp. 930-933, 2008.
- [12] T. J. Yorkey, J. G. Webster, and W. J. Tompkins, "Comparing reconstruction algorithms for electrical impedance tomography," *IEEE Transactions on Biomedical Engineering*, vol. 34, no. 11, pp. 843-852, 1987.
- [13] A. N. Tikhonov, "Solution of incorrectly formulated problems and the regularization method," *Soviet Math Dokl*, vol. 4, pp. 1035-1038, English translation of Dokl Akad Nauk SSSR, vol. 151, pp. 501-504, 1963.
- [14] P. Hua, J. G. Webster, and W. J. Tompkins, "A regularised electrical impedance tomography reconstruction algorithm," *Clin. Phys. Physiol. Meas.*, vol. 9(A), pp. 137-141, 1988.
- [15] P. Hua, E. J. Woo, J. W. Webster, and W. J. Tompkins, "Iterative reconstruction methods using regularization and optimal current patterns in electrical impedance tomography," *IEEE Trans. Med. Imag.*, vol. 10, pp. 621-628, 1991.
- [16] D. C. Dobson and F. Santosa, "An image enhancement technique for electrical impedance tomography," *Inverse Prob.*, 10, pp. 317-334, 1994.
- [17] A. Borsic, R. B. Lionheart, and N. McLeod, "Generation of anisotropic-smoothness regularization filters for EIT," *IEEE Transactions on Medical Imaging*, vol. 21, no. 6, pp. 579-587, 2002.
- [18] N. J. Avis and D. C. Barber, "Image reconstruction using non-adjacent drive configurations," *Physiol. Meas.*, vol. 15, pp. 153-160, 1994.
- [19] A. Adler and W. R. B. Lionheart, "Uses and abuses of EIDORS: an extensible software base for EIT," *Physiol. Meas.*, vol. 27, pp. 25-42, 2006.
- [20] M. J. Ackerman, "The visible human project," *Proc. IEEE*, vol. 86, no. 3, pp. 504-511, 1998.
- [21] D. Andreuccetti, R. Fossi, and C. Petrucci, *An internet resource for the calculation of the dielectric properties of body tissues in the frequency range 10 Hz - 100 GHz*, Internet document; URL: <http://niremf.ifac.cnr.it/tissprop/>
- [22] G. d'Inzeo, C. Giacomozzi, and S. Pisa, "Analysis of the stimulation of a nerve fiber surrounded by an inhomogeneous, anisotropic, and dispersive tissue," *Applied Computational Electromagnetics Society Journal*, vol. 7, no. 2, pp. 179-190, 1992.
- [23] G. H. Golub and C. F. Van Loan, *Matrix Computation*. 4rd ed., The Johns Hopkins University Press, Baltimore, 2013.
- [24] J. Goble, M. Cheney, and D. Isaacson, "Electrical impedance tomography in three dimensions," *Applied Computational Electromagnetics Society Journal*, vol. 7, no. 2, pp. 128-147, 1992.
- [25] J. C. Tozer, R. H. Ireland, D. C. Barber, and A. T. Barker, "Magnetic impedance tomography," *Ann. N. Y. Acad. Sci.*, vol. 873, pp. 353-359, Apr. 1999.
- [26] L. Hao and L. Xu, "Joint L1 and total variation regularization for magnetic detection electrical impedance tomography," *Applied Computational Electromagnetics Society Journal*, vol. 31, no. 6, pp. 677-683, June 2016.
- [27] V. Sarode, S. Patkar, and A. N. Cheeran, "Comparison of 2-D algorithms in EIT based image reconstruction," *Int. Journal of Computer Applications*, vol. 8, pp. 6-11, 2013.
- [28] B. Grychtol, G. Elke, P. Meybohm, N. Weiler, I. Frerichs, and A. Adler, "Functional validation and comparison framework for EIT lung imaging," *PLoS ONE*, vol. 9, pp. 1-13, 2014.
- [29] A. Adler, J. H. Arnold, R. Bayford, A. Borsic, B. Brown, P. Dixon, T. J. C. Faes, I. Frerichs, H. Gagnon, Y. Garber, B. Grychtol, G. Hahn, W. R. B. Lionheart, A. Malik, R. P. Patterson, J. Stocks, A. Tizzard, N. Weiler, and G. K. Wolf, "GREIT: A unified approach to 2D linear EIT reconstruction of lung images," *Physiol. Meas.*, vol. 30, pp. 169-191, 2009.
- [30] A. Tizzard, L. Horesh, R. J. Yerworth, D. S. Holder, and R. H. Bayford, "Generating accurate finite element meshes for the forward model of the human head in EIT," *Physiol. Meas.*, vol. 26, pp. 251-261, 2005.
- [31] W. R. Breckon and M. K. Pidcock, "Some mathematical aspects of electrical impedance tomography," *Mathematics and Compute Science in Medical*

Imaging, ed. M. A. Viergever and A. E. Todd-Pokropek (Berlin: Springer), pp. 204-215, 1988.

- [32] F. Grunberg "Respiratory cycle in 90 images," *Drager Review*, vol. 99, no. 1, Feb. 2010.



Stefano Pisa received the Electronic Engineering and Ph.D. degrees from the University of Rome "La Sapienza," Rome, Italy, in 1985 and 1988, respectively. In 1989, he joined the Department of Electronic Engineering, University of Rome "La Sapienza," as a Researcher. Since 2001, he has been an Associate Professor with the same university. His research interests are the interaction between electromagnetic fields and biological systems, therapeutic and diagnostic applications of electromagnetic fields, and the modeling and design of MW circuits. He has authored over 150 scientific papers and numerous invited presentations at international workshops and conferences. Pisa is a Member of the IEEE Microwave Theory and Techniques Society. He serves as a Reviewer for different international journals.



Erika Pittella received the M.S. (cum laude) and Ph.D. degrees in Electronic Engineering from the Sapienza University of Rome, Rome, Italy, in 2006 and 2011, respectively. She is currently a Research Associate with the Department of Information Engineering, Electronics and Telecommunications, Sapienza University of Rome. Pittella's research interests are electromagnetism applied to medicine, main research activities are related to the modeling of ultra wideband radars for the remote monitoring of cardiorespiratory activity, to the design of sources, antennas, and receivers of such systems, and the measurement of dielectric characteristics of materials. She is also interested in dosimetric aspects of the interaction between electromagnetic fields radiated by ultra wideband radar systems and exposed subjects. Pittella is a Member of the IEEE Instrumentation and Measurement Society, and of the Italian Group of Electrical and Electronic Measurements (GMEE). She serves as a Reviewer for different international journals.



Emanuele PiuZZi received the M.S. (cum laude) and Ph.D. degrees in Electronic Engineering from Sapienza University of Rome, Rome, Italy, in 1997 and 2001, respectively. He is currently an Assistant Professor of Electrical and Electronic Measurements with the Department of Information Engineering, Electronics and Telecommunications, Sapienza University of Rome. He is the co-author of over 100 publications. His current research interests include the measurement of complex permittivity of materials, time domain reflectometry applications, biomedical instrumentation design, and evaluation of human exposure to electromagnetic fields. PiuZZi is a Member of the IEEE Instrumentation and Measurement Society, of the Italian Group of Electrical and Electronic Measurements (GMEE), and of the Italian Electrotechnical Committee (CEI). He serves as a Reviewer for different international journals.